RSC Advances

PAPER

Check for updates

Ti₃C₂ MXene: a promising microwave absorbing material

Wanlin Feng,†[a] Heng Luo,†[b] Yu Wang,[a] Sifan Zeng,[a] Lianwen Deng,[b] Xiaosong Zhou,[a] Haibin Zhang (ID) *[a] and Shuming Peng*[a]

In this work, we demonstrate the enhancement of microwave attenuation capability of Ti₃C₂ enabled microwave absorbing materials (MAMs) within a frequency range of 2–18 GHz. Ti₃C₂ nano-sheet/paraffin composites exhibit enhanced microwave absorbing performance with an effective absorbing bandwidth of 6.8 GHz (11.2–18 GHz) at 2 mm and an optimal reflection loss of −40 dB at 7.8 GHz. Moreover, mechanisms for the dielectric responses of the Ti₃C₂ MXene nanosheets are intensively discussed. Three typical electric polarizations of Ti₃C₂ are illustrated with the Cole–Cole diagram. The enhanced microwave absorbing properties can be ascribed to the high dielectric loss accompanied with the strong multi-reflections between MXene layers.

1. Introduction

Driven by the demand for eliminating the adverse effects of electromagnetic waves (EMWs), more and more effort has been devoted to the development of light weight and high performance electromagnetic interference (EMI) shielding and/or absorbing materials. Among them, carbon-based materials have been widely studied as good electromagnetic interference (EMI) shielding and/or absorbing materials.[1–6] The last decades have witnessed intensive interest towards carbonaceous filler enabled polymer composites.[7–9] Recently, Shahzad F. *et al.*[10] reported a Ti₃C₂Tₓ film with an outstanding EMI shielding effectiveness of 92 dB, and demonstrated the considerable potential of a new two-dimensional family: MXenes[11] and their polymer composites for EMI shielding application.

However, EMI shielding materials mainly focus on the reflection of radiation using charge carriers which could interact with incident electromagnetic waves directly. But the reflected radiation could still have adverse effects on the surroundings and electrical devices.[12–14] Therefore, electromagnetic wave absorbing materials (MAMs) with reduced reflections and enhanced internal attenuations are considered to be more competitive candidates for EMI. With the development of graphene[15,16] and graphene-based composites,[17–21] two dimensional microwave absorbing materials have gained more and more attention, owing to their enhanced multi-internal-reflections, low density and superior mechanical flexibility. Recent years, a novel family of electrical conductive two-dimensional transition metal carbide/nitride labeled as MXene,[11] have been demonstrated to be popular alternatives for MAMs, due to laminated morphologies, unique mechanical and electronic properties.[22,23]

Ti₃C₂ is a representative among the big MXene family. Owing to the laminated morphology and unique combination of metallic conductivity and hydrophilicity, Ti₃C₂ has been widely studied to be as attractive candidates for energy storage devices,[24–28] catalysts,[29] sensors,[30] electromagnetic interference (EMI) shielding materials[31] and microwave absorbing materials.[32–34] Besides, as demonstrated previously,[35–37] microwave absorbers with flake-shaped fillers exhibit superior microwave absorption performance compared to those with spherical fillers. Therefore, it is reasonable to assume that the MXenes with two-dimensional nanocrystals have a great potential for application in MAMs. Nevertheless, exploration on underlying mechanism of dielectric behaviors for this novel MAMs with Ti₃C₂ is urgently needed.

Herein, we demonstrate the enhancement of microwave attenuation capability of Ti₃C₂ enabled MAMs within frequency range of C-band (4–8 GHz), X-band (8–12 GHz) and Ku-band (12–18 GHz). Moreover, mechanisms of dielectric responses for MAMs filled with Ti₃C₂ nanosheets are intensively discussed. These findings point to important guidelines to reveal underlying mechanism of electromagnetic responses for Ti₃C₂ composites, which is beneficial to regulation for microwave absorption performance of MXene functionalized absorber including but not limited to Ti₃C₂ composites, and pave the way for the development of novel MAMs.

[a]Innovation Research Team for Advanced Ceramics, Institute of Nuclear Physics and Chemistry, China Academy of Engineering Physics, Mianyang, 621900, China. E-mail: hbzhang@caep.cn; pengshuming@caep.cn

[b]School of Physics and Electronics, Institute of Super-microstructure and Ultrafast Process in Advanced Materials, Central South University, Changsha, 410083, China

† W. L. Feng and H. Luo contributed equally to this work.

2. Experimental

2.1. Sample preparation

As starting materials, commercially available titanium, aluminum and carbon powders (purity > 95%, $d_{50} = 30$ μm), were kindly provided by Forsman Scientific (Beijing) Co., Ltd., and were used to prepared Ti_3AlC_2 powders through pressure-less sintering at 1560 °C for 1 h. After that, Ti_3AlC_2 powders were immersed in 49 wt% aqueous HF at ambient temperature in an ultrasonic homogenizer for 4 h. The as-derived Ti_3C_2 MXene nanopowders were separated by centrifuge and washed with distilled water until pH ≈ 6.

2.2. Characterization

Phase analysis was conducted on X-ray diffractometer (XRD, X′ Pert PRO, Netherlands) using Cu Kα radiation ($\lambda = 0.1546$ nm) and a step scan of 0.02° with 1 s per step from 5–65 degree (the typical XRD peaks of original Ti_3AlC_2 and derived Ti_3C_2 MXene are among 5–65 degrees), operating at 40 kV and 20 mA, respectively, data analysis with Jade software. A scanning electron microscope (SEM, Quanta 400, FEI, America), with an accelerating voltage of 20 kV was used to obtain micro-morphology images of derived Ti_3C_2 MXene flakes and conduct elemental analysis *via* energy-dispersive X-ray (EDX) spectroscopy. A transmission electron microscope (TEM, HT7700, HITACHI, Japan), with an accelerating voltage of 120 kV was also used to obtain high-magnification images of MXene sheets. For the characterization of dielectric responses ranging from 2 GHz to 18 GHz, donut-shaped samples with 7.0 mm outer diameter and 3.0 mm inner diameter were prepared by mixing the as-prepared Ti_3C_2 MXene powders with molten paraffin (weight ratio equals to 1 : 1), and the electromagnetic (EM) parameters (relative permittivity ε_r and permeability μ_r) of each samples was determined through coaxial line method with a vector network analyzer (Agilent AV3618). All the measurements were carried out at room temperature. For accuracy of measurement, the system is carefully calibrated with Short-Open-Load-Through (SOLT) approach. Based on theory of transmission lines,[38–40] the reflection loss (RL) of a metal-backed absorber with ε_r and μ_r could be expressed as:

$$R(\mathrm{dB}) = 20 \log \left| \frac{Z_{\mathrm{in}} - 1}{Z_{\mathrm{in}} + 1} \right| \qquad (1)$$

and

$$Z_{\mathrm{in}} = \sqrt{\frac{\mu_r}{\varepsilon_r}} \tanh \left[\mathrm{j} \left(\frac{2\pi}{c} \right) \sqrt{\mu_r \varepsilon_r} f d \right] \qquad (2)$$

where Z_{in} refers to input impedance, j is the imaginary unit (*i.e.* equals to $\sqrt{-1}$), c is the velocity of electromagnetic waves in free space, f is the microwave frequency, and d is the thickness of the samples.

3. Results and discussion

The pressureless-sintered Ti_3AlC_2 powders are phase-pure as determined by XRD showing in Fig. 1. After subjected to HF and
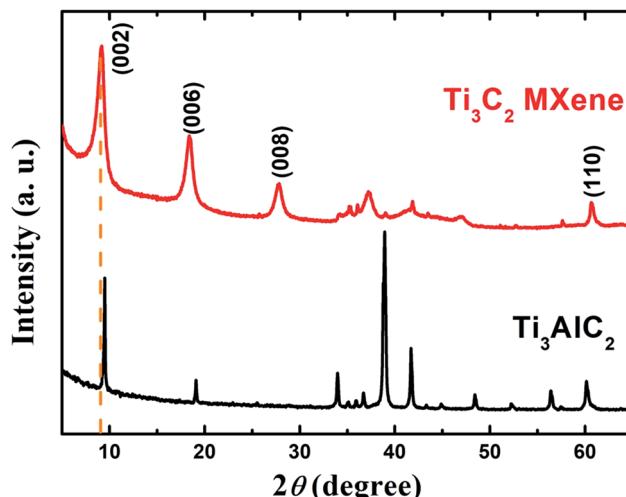
Fig. 1 XRD patterns of pressureless-sintered Ti_3AlC_2 and as-derived Ti_3C_2 MXene.

ultrasonic treat, the characteristic peaks within range of 33° to 43° of Ti_3AlC_2 eventually vanish as expected. In addition, the (002) peaks of Ti_3C_2 MXene are inclined to shift towards smaller angle and be broadened compared to that of Ti_3AlC_2,[11] owing to successful extraction of Al-atoms from Ti_3AlC_2. The above changes are widely recognized the formation of MXene, and the vanish of 39°(104) peak reveals the exhaustion of Ti_3AlC_2 and confirms that the derived MXene is phase pure.

The cross-sectional SEM image of Ti_3C_2 which illustrated in Fig. 2a suggests that the accordion-like Ti_3C_2 nanosheets keep stacked after etching of Ti_3AlC_2, and the inter-lamellar spacing between Ti_3C_2 nanosheets is estimated to be around 1 nm by cross-sectional TEM observation (Fig. 2c), which is accordant with calculated result of 0.98 nm corresponding to (002) peak of XRD pattern. EDS spectrum (Fig. 2b) reveals that MXene is composed of Ti, C, O, F, and little Al. Fig. 2d shows a two-layer Ti_3C_2 flakes, which is thin enough to be electron-transparent.

It should be noted that the Ti_3C_2 MXene in this work was synthesized by a fierce chemical reaction of Ti_3AlC_2 and hydrofluoric acid (HF), and the derived MXene sheets were combined together with hydrogen bonds.[11] The fierce etching by HF not only extracted Al atoms from Ti_3AlC_2, but also eaten off some of Ti atoms, which created abundant intrinsic defects. The hydrogen bond is a weak chemical bond between an electronegative atom, such as fluorine, oxygen, or nitrogen, and a hydrogen atom bound to another electronegative atom, which is different from the traditional strong interaction of chemical bonds. Based on the two aspects above, the derived Ti_3C_2 MXene is not a perfect crystal structure, but between crystal and amorphous structure and full of intrinsic defects. The unique microstructure of Ti_3C_2 MXene, which corresponding to the broadening of XRD peaks, is supposed to have an impact on the dielectric behaviors and microwave absorption capability.

It is well recognized that most majority of microwave attenuation materials are frequency dependent, that dependence constrains the values the real and imaginary parts of the relative permittivity ($\varepsilon = \varepsilon' - \mathrm{j}\varepsilon''$) and relative permeability ($\mu = \mu' - \mathrm{j}\mu''$)
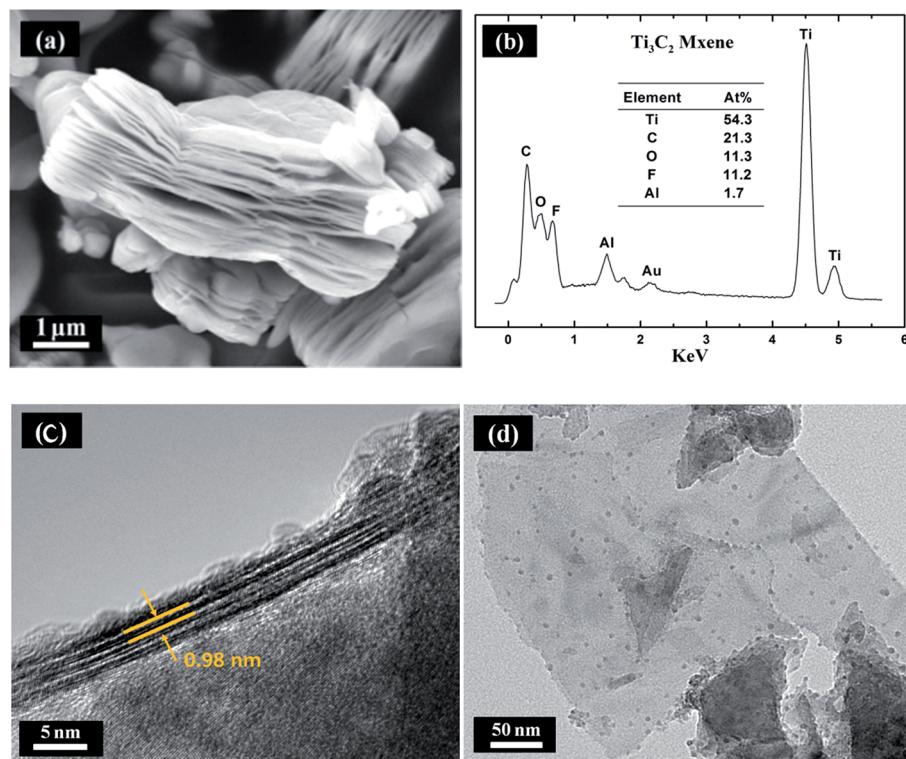
Fig. 2 (a) Cross-section SEM image of Ti_3C_2 particles; (b) EDS spectrum of Ti_3C_2 MXene, revealing the chemical composition of MXene; (c) cross-section TEM image of a 4-layer Ti_3C_2 flake, the estimated inter-layer space is about 1 nm; (d) TEM image of a 2-layer Ti_3C_2 flake.

can take. As illustrated in Fig. 3a, both ε' and ε'' of composites filled with 50 wt% Ti_3C_2 MXene exhibit frequency dispersion effect, while the μ maintains at around $1 - j \cdot 0$. Therefore, Ti_3C_2 MXene is considered to be a typical dielectric loss material. Fig. 3b shows the reflection loss (RL) over 2–18 GHz at three typical values of thickness. The RL keeps lower than -10 dB within the whole Ku-band (12.4–18 GHz) when the thickness of absorber is only 2 mm, which suggests more than 90% of energy of incident electromagnetic wave have been absorbed. Besides, an optimal RL of -40 dB (corresponding to 99.94% absorption) could be achieved at 7.8 GHz. This superior microwave attenuation capability demonstrates Ti_3C_2 MXene to be a promising candidate for lightweight stealth materials.

In addition, with the help of quarter-wavelength absorption,[41] the absorption peak is inclined to shift from 12.5 GHz to 6 GHz and absorption band (RL < -5 dB) improves significantly within frequency range of less than 8 GHz, when thickness of absorber increased from 2 mm to 4 mm. According to the resonant absorb theory, when microwave is incident on an absorber sample backed by a perfect conductor, the predicted matching thickness d at the matching frequency f is given by:

$$f = \frac{c}{4d\left(\sqrt{|\mu(f)\varepsilon(f)|}\right)} \quad (3)$$

where $\mu(f)$ and $\varepsilon(f)$ are complex permeability and permittivity at the frequency of f, respectively.
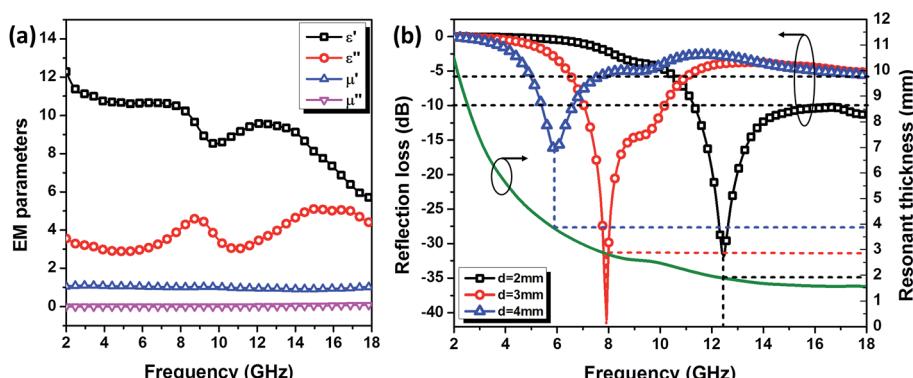
**Fig. 3** (a) Dielectric and (b) microwave absorbing properties of Ti_3C_2 nano-sheets/paraffin composites.

Apparently based on eqn (3), the attenuation peaks are supposed to shift to lower frequency with increasing sample thickness, and are well consistent with the predicted reflection loss curves (see Fig. 3b). All these results indicate that, in addition to the intrinsic loss originated from dielectric relaxation, quarter-wavelength absorption is also one of effective way to improve microwave absorption for the Ti_3C_2 MXene nanosheets filled composites. It should be noticed here that the enhanced microwave absorbing performance at low frequencies makes Ti_3C_2 MXene composites competitive in field of light weight MAMs.

Conventionally the relaxation process which can be described by the Cole–Cole semicircle has an important influence on permittivity behaviors of microwave absorbing materials. As clearly illustrated in Fig. 4, experimental points of permittivity of Ti_3C_2 MXene composites in Cole–Cole plane are inclined to distribute on three distinguishable sections of circular arc with the help of nonlinear fitting. This fact suggests the supposed existence of three types of electric polarization and relaxation.

Ti_3C_2 MXene nanosheets are highly electrical conductive,[42] and there exists migration of free electrons inside the sheets, as well as charge accumulation at interfaces between MXene sheets and insulated matrix (here refers to paraffin) when subjected to external electric field, which is considered to be the fundamental mechanism of dielectric polarization. The electric polarization could be grouped into three types which are marked as I, II and III respectively (see in Fig. 4). For the type I, two localized charge layers in neighboring MXene sheets with opposite charge, which generally referred to as interfacial polarization or Maxwell–Wagner polarization,[43] are supposed to play the roles of electrodes in 'mico-capacitances'. It is well established that the dielectric behavior for interfacial polarization could be described by the Debye equation:[44]

$$\left(\varepsilon' - \frac{\varepsilon_s + \varepsilon_\infty}{2}\right)^2 + (\varepsilon'')^2 = \left(\frac{\varepsilon_s - \varepsilon_\infty}{2}\right)^2 \qquad (4)$$

where ε_s and ε_∞ are 'static' and 'infinite frequency' dielectric constant, respectively. Eqn (4) suggests that the locus of permittivity in the Cole–Cole plane should be a semicircle with centered on the ε' axis, which is accordant with the experimental results.

Type II describes the electric polarization in a certain nanosheet along the direction of lamella (*i.e.* in the *ab* plane). Due to the charge accumulation at two ends of sheets, MXene nanosheets are more inclined to be equivalent to 'micro-dipoles'. And the scattering effect of crystal lattice on the back-and-forth movement of electrons under alternating EM wave, which results in thermal energy, predominately contributes to the dissipation of EM energy. Furthermore, there exists alternating conduction current in the *ab* plane of MXene nanosheets under alternating EM wave, owning to the Ti–Ti metallic bonding.[42] Taking these into consideration brings the Debye equation (eqn (4)) into more empirical and described by:

$$\varepsilon = \varepsilon_\infty + \frac{\varepsilon_s - \varepsilon_\infty}{1 + j\omega\tau} - j\left(\frac{\sigma}{\omega\varepsilon_0}\right) \qquad (5)$$

where τ refers to relaxation time, ω is angular frequency of EM wave, ε_0 is permittivity of vacuum (8.85×10^{-12} F m^{-1}), and σ is the conductivity. After decomposition of eqn (5) into the real and imaginary parts, the relationship between ε' and ε'' could be expressed as:

$$\left(\varepsilon' - \frac{\varepsilon_s + \varepsilon_\infty}{2}\right)^2 + \left(\varepsilon'' - \frac{\sigma}{\omega\varepsilon_0}\right)^2 = \left(\frac{\varepsilon_s - \varepsilon_\infty}{2}\right)^2 \qquad (6)$$

Apparently, the locus of dielectric behavior for type II according to eqn (6) should still be a circle, however, whose center is supposed to locate in the first quadrant (see circle 3 in
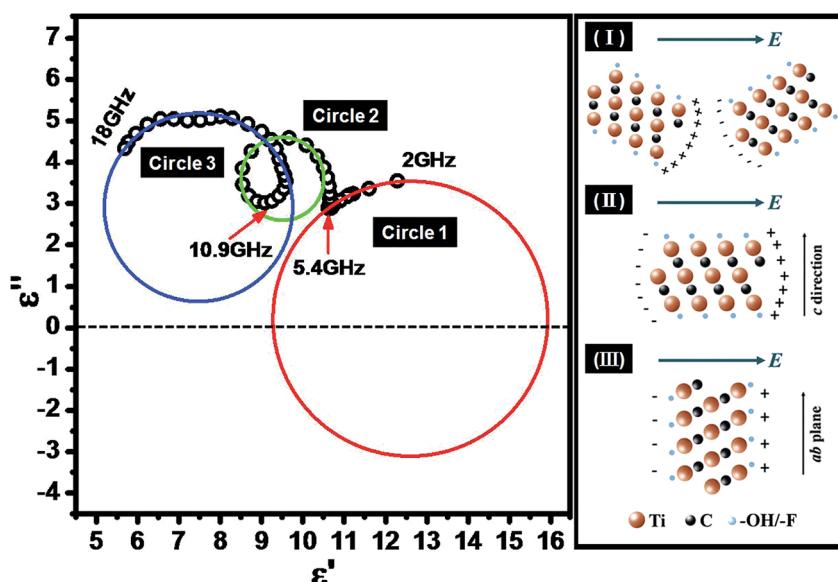

Fig. 4 Typical Cole–Cole diagram over 2–18 GHz and three typical electric polarization in Ti_3C_2 composites.

Fig. 4). Note that the vibration of terminations T_x (–OH/–F), which located on the surface of Ti_3C_2 MXene nanosheets, is also supposed to make a contribution to microwave absorption capability under alternating EM wave (see circle 1 in Fig. 4). Moreover, due to the strong Ti–C bond, the electrical conductivity along the c direction is much lower than that in the ab plane.[42] As a result, it is reasonable to assume that the electric polarization along the c direction, which referred to as type III, could be neglected compared with that in ab plane which discussed above.

In addition, multiple reflections and scattering between Ti_3C_2 MXene layers could also further enhance the microwave absorbing ability.[45] Another important feature should be noticed is that the transition points for three segments of circular arc in Fig. 4, corresponding to three types of electric polarization discussed above, locate at 5.4 GHz and 10.9 GHz, respectively. If shifting attentions back to the reflection loss of Ti_3C_2 MXene composites which illustrated in Fig. 3b, it is tempting to see that the superior microwave attenuation capability mainly focuses on high frequency especially exceeded 10.9 GHz, while reflection loss of Ti_3C_2 MXene composites seems difficult to be lower than −10 dB within frequency range of lower than 5.4 GHz even thickness of absorber reaches 4 mm. As a consequence, it is legitimate to conclude that intrinsic electric polarization and relaxation loss within Ti_3C_2 MXene nanosheets as well as quarter-wavelength absorption play a dominate role of excellent dissipation capability for microwave energy.

4. Conclusion

Ti_3C_2 is successfully synthesized by etching pressureless-sintered Ti_3AlC_2 in HF under ultrasonic circumstance. The as-derived Ti_3C_2 nano-sheets/paraffin composites exhibit enhanced microwave absorbing performance with an effective absorbing bandwidth of 6.8 GHz (11.2–18 GHz) at 2 mm and an optimal reflection loss of −40 dB at 7.8 GHz. Moreover, mechanisms of dielectric responses for Ti_3C_2 nanosheets are intensively discussed. Three typical electric polarization in Ti_3C_2 composites are illustrated with the Cole–Cole diagram. The enhanced microwave absorbing properties can be ascribed to the high dielectric loss accompanied with the strong multi-reflections between MXene layers. These findings point to important guidelines to reveal underlying mechanism of electromagnetic responses for Ti_3C_2 MXene composites, which is beneficial to regulation for microwave absorption performance of MXene functionalized absorbers.

Conflicts of interest

There are no conflicts to declare.

Acknowledgements

References

1 M. H. Al-Saleh, W. H. Saadeh and U. Sundararaj, *Carbon*, 2013, **60**, 146–156.

2 Z. Fan, G. Luo, Z. Zhang, L. Zhou and F. Wei, *Mater. Sci.Eng. B*, 2006, **132**, 85–89.

3 J. M. Thomassin, D. Vuluga, M. Alexandre, C. Jérôme, I. Molenberg, I. Huynen and C. Detrembleur, *Polymer*, 2012, **53**, 169–174.

4 L. Deng and M. Han, *Appl. Phys. Lett.*, 2007, **91**, 354.

5 B. Shen, Y. Li, D. Yi, W. Zhai, X. Wei and W. Zheng, *Carbon*, 2016, **102**, 154–160.

6 T. Zou, C. Shi and N. Zhao, *J. Mater. Sci.*, 2006, **42**, 4870–4876.

7 D. Zhao, J. Zhang, X. Li and Z. Shen, *J. Alloys Compd.*, 2010, **505**, 712–716.

8 N. Li, Y. Huang, F. Du, X. He, X. Lin and H. Gao, *Nano Lett.*, 2006, **6**, 1141–1145.

9 B. Wen, M. Cao, M. Lu, W. Cao, H. Shi, J. Liu, X. Wang, H. Jin, X. Fang, W. Wang and J. Yuan, *Adv. Mater.*, 2014, **26**, 3484–3489.

10 F. Shahzad, M. Alhabeb, C. B. Hatter, B. Anasori, S. Man Hong, C. M. Koo and Y. Gogotsi, *Science*, 2016, **353**, 1137–1140.

11 M. Naguib, M. Kurtoglu, V. Presser, J. Lu, J. Niu, M. Heon, L. Hultman, Y. Gogotsi and M. W. Barsoum, *Adv. Mater.*, 2011, **23**, 4248–4253.

12 T. Liu, Y. Pang, M. Zhu and S. Kobayashi, *Nanoscale*, 2014, **6**, 2447.

13 Z. Liu, G. Bai, Y. Huang, F. Li, Y. Ma, T. Guo, X. He, X. Lin, H. Gao and Y. Chen, *J. Phys. Chem. C*, 2007, **111**, 13696.

14 Y. Zhang, Y. Huang, T. Zhang, H. Chang, P. Xiao, H. Chen, Z. Huang and Y. Chen, *Adv. Mater.*, 2015, **27**, 2049.

15 K. S. Novoselov, A. K. Geim, S. V. Morozov, D. Jiang, Y. Zhang, S. V. Dubonos, I. V. Grigorieva and A. A. Firsov, *Science*, 2004, **306**, 666–669.

16 H. Gao, Z. Liu and X. Feng, *Small*, 2014, **10**, 2121.

17 C. Hu, Z. Mou, G. Lu, N. Chen, Z. Dong, M. Hu and L. Qu, *Phys. Chem. Chem. Phys.*, 2013, **15**, 13038.

18 X. Zheng, J. Feng, Y. Zong, H. Miao, X. Hu, J. Bai and X. Li, *J. Mater. Chem. C*, 2015, **3**, 4452.

19 L. Wang, Y. Huang, X. Sun, H. Huang, P. Liu, M. Zong and Y. Wang, *Nanoscale*, 2014, **6**, 3157.

20 D. Sun, Q. Zou, Y. Wang, Y. Wang, W. Jiang and F. Li, *Nanoscale*, 2014, **6**, 6557.

21 P. B. Liu, Y. Huang, J. Yan and Y. Zhao, *ACS Appl. Mater. Interfaces*, 2016, **8**, 5536.

22 M. Naguib, V. N. Mochalin, M. W. Barsoum and Y. Gogotsi, *Adv. Mater.*, 2014, **26**, 992–1005.

23 O. Mashtalir, M. Naguib, V. N. Mochalin, Y. Dall'Agnese, M. Heon, M. W. Barsoum and Y. Gogotsi, *Nat. Commun.*, 2013, **4**, 1716.

24 M. Naguib, J. Halim, J. Lu, K. M. Cook, L. Hultman, Y. Gogotsi and M. W. Barsoum, *J. Am. Chem. Soc.*, 2013, **135**, 15966–15969.

25 D. Er, J. Li, M. Naguib, Y. Gogotsi and V. B. Shenoy, *ACS Appl. Mater. Interfaces*, 2014, **6**, 11173–11179.

26 M. Ghidiu, M. R. Lukatskaya, M. Q. Zhao, Y. Gogotsi and M. W. Barsoum, *Nature*, 2014, **516**, 78–81.

27 X. Wang, S. Kajiyama, H. Iinuma, E. Hosono, S. Oro, I. Moriguchi, M. Okubo and A. Yamada, *Nat. Commun.*, 2015, **6**, 6544.

28 M. R. Lukatskaya, O. Mashtalir, C. E. Ren, Y. Dall'Agnese, P. Rozier, P. L. Taberna and M. Naguib, *Science*, 2013, **341**, 1502–1505.

29 J. Ran, G. Gao, F. T. Li, T. Y. Ma, A. Du and S. Z. Qiao, *Nat. Commun.*, 2017, **8**, 13907.

30 J. Chen, K. Chen, D. Tong, Y. Huang, J. Zhang, J. Xue, Q. Huang and T. Chen, *Chem. Commun.*, 2015, **51**, 314–317.

31 M. A. Faisal Shahzad, C. B. Hatter, B. Anasori, S. M. Hong, C. M. Koo and Y. Gogotsi, *Science*, 2016, **353**, 1137–1140.

32 Q. Yuchang, Z. Wancheng, L. Fa and Z. Dongmei, *Ceram. Int.*, 2016, **7**, 150.

33 X. Y. Meikang Han, X. Li, B. Anasori, L. Zhang, L. Cheng and Y. Gogotsi, *ACS Appl. Mater. Interfaces*, 2017, **9**, 20038–20045.

34 M. Han, X. Yin, H. Wu, Z. Hou, C. Song, X. Li, L. Zhang and L. Cheng, *ACS Appl. Mater. Interfaces*, 2016, **8**, 21011–21019.

35 R. B. Yang, W. F. Liang, S. T. Choi and C. K. Lin, *IEEE Trans. Magn.*, 2013, **49**, 4180–4183.

36 J. Wei, T. Wang and F. Li, *J. Magn. Magn. Mater.*, 2011, **323**, 2608–2612.

37 Y. Qing, W. Zhou, F. Luo and D. Zhu, *Ceram. Int.*, 2016, **42**, 16412–16416.

38 Z. Peng, J. Y. Hwang and M. Andriese, *Ceram. Int.*, 2013, **39**, 6721–6725.

39 M. S. Cao, W. L. Song, Z. L. Hou, B. Wen and J. Yuan, *Carbon*, 2010, **48**, 788–796.

40 R. C. Che, L. M. Peng, X. F. Duan, Q. Chen and X. L. Liang, *Adv. Mater.*, 2004, **16**, 401–405.

41 P. Xu, X. Han, J. Jiang, X. Wang, X. Li and A. Wen, *J. Phys. Chem. C*, 2007, **111**, 12603–12608.

42 Y. C. Zhou, X. H. Wang, Z. M. Sun and S. Q. Chen, *J. Mater. Chem.*, 2001, **11**, 2335–2339.

43 L. Y. Yeo, D. Lastochkin, S.-C. Wang and H. C. Chang, *Phys. Rev. Lett.*, 2004, **92**, 133902.

44 J. Feng, F. Pu, Z. Li, X. Li, X. Hu and J. Bai, *Carbon*, 2016, **104**, 214–225.

45 X. Sun, J. He, G. Li, J. Tang, T. Wang, Y. Guo and H. Xue, *J. Mater. Chem. C*, 2013, **1**, 765–777.